Ringdown cavity absorption spectroscopy of the very weak HCN overtone bands with six, seven, and eight stretching quanta

D. Romanini and K. K. Lehmann

Citation: The Journal of Chemical Physics **99**, 6287 (1993); doi: 10.1063/1.465866
View online: http://dx.doi.org/10.1063/1.465866
View Table of Contents: http://scitation.aip.org/content/aip/journal/jcp/99/9?ver=pdfcov
Published by the AIP Publishing

Ring-down cavity absorption spectroscopy of the very weak HCN overtone bands with six, seven, and eight stretching quanta

D. Romanini and K. K. Lehmann
Department of Chemistry, Princeton University, Princeton, New Jersey 08544-1009

(Received 23 November 1992; accepted 22 July 1993)

A nonstandard, high sensitivity, absorption detection technique has been applied to the investigation of the very weak fifth, sixth, and seventh overtones of HCN at 100 Torr and 296 K. The frequency range covered is from 17 500 to 23 000 cm^{-1}. We report high resolution, absolute absorption spectra with a noise equivalent sensitivity as low as $\sim 2\times 10^{-9}$/cm (recently improved to 7×10^{-10}/cm). Band origins, rotational constants, and band intensities are reported and compared with calculated values. The HCN overtone spectra in the present study are not affected by any kind of perturbation, despite the high excitation energy involved.

I. INTRODUCTION

Highly excited molecular states probe the portion of the intramolecular potential which is relevant to molecular dynamics and related phenomena, such as unimolecular reactions and internal vibrational redistribution. Comparison of the measured position and of the intensity of each state with calculated values constitutes complementary tests to the efficacy of the theoretical model and approximations employed. The positions of the vibrational states are sensitive to different portions of the intramolecular potential surface, while their intensities are determined by the dipole moment surface and are especially sensitive to the repulsive wall of the potential.[1]

For hydrogen cyanide and a number of its isotopomers, extensive experimental data are available up to relatively high excitation energies. The HCN overtone spectra with up to six stretching quanta (up to 18 500 cm^{-1}) have been thoroughly characterized using photoacoustic and white-cell absorption spectroscopies.[2–6] Diode laser spectra of the first CH stretch overtone have also been reported by Sasada *et al.*[7] More recently, spontaneous emission pumping has been used to study HCN overtones involving high bending excitation by Yang, Rogaski, and Wodtke.[8] Together with the new results reported here, HCN is probably the molecule with the most extensively characterized vibrational spectrum. Good agreement has been found between our data and calculations by Carter *et al.*[9] for the band origins, and by Botschwina[10] for the intensities.

We have used a relatively new technique,[11] the ring-down cavity, to detect HCN overtone bands with seven and eight quanta of stretching excitation 205, 106, 007, 305, 206, and 107. The convention we use for the vibrational quantum numbers is (CN stretch) (bend) (CH stretch). In terms of sensitivity, this technique is comparable to the photoacoustic spectroscopy, but it has the advantage of allowing a direct and accurate absolute spectral intensity determination. For this reason, we have revisited the 006 and 105 HCN overtone bands in an attempt to resolve a controversy involving their intensities. Our measurements do not support the unusually high 105 intensity previously reported by Smith *et al.*[4] Instead, the 105 intensity that we obtain fits in the trend followed by the other overtones and agrees with the results of *ab initio* calculations by Botschwina.[10,12] It should be emphasized that with these new results, the HCN overtone absolute intensity data cover most of the visible spectrum. Consequently, this molecule becomes a very convenient intensity calibration standard for other high sensitivity techniques such as the photoacoustic spectroscopy.

Considering the relative novelty of the ring-down cavity absorption detection scheme and the strong likelihood that its use will become more widespread in the near future, it is necessary to give a very detailed account of our experimental arrangement. This description will also highlight some relevant improvements with respect to previous ones.[11] In addition, we will discuss the origin of the observed noise level (and its theoretical lower limit) and the cause of the baseline etaloning that in certain conditions can affect ring-down cavity (RDC) spectra.

II. EXPERIMENT

The RDC absorption detection scheme can achieve a sensitivity (our best value is $\sim 7\times 10^{-10}$/cm) comparable to that of a resonant photoacoustic cell, with the considerable advantage of a direct and accurate determination of the absolute absorption intensity. In RDC spectroscopy, the photon decay time inside a high quality optical resonator is measured as a function of frequency. This decay time is inversely proportional to the resonator losses. Since the losses of the bare resonator cavity are extremely low, very weak absorption due to a sample inserted in the cavity can be detected. With a RDC setup, a "noisy" pulsed dye laser can be used to perform absorption measurements with a sensitivity of better than 1% over an "effective path length" that corresponds to the RDC photon decay time (multiplying by the speed of light). The best effective absorption path length that we could recently achieve is 70 km. For the measurements reported in this paper, the path length varied from 5 to 20 km.

To our knowledge, the technique in the present form (in particular, with respect to the pulsed nature of the laser system) has been pioneered by O'Keefe and Deacon[11] in 1988 by detecting very weak absorption bands in gaseous

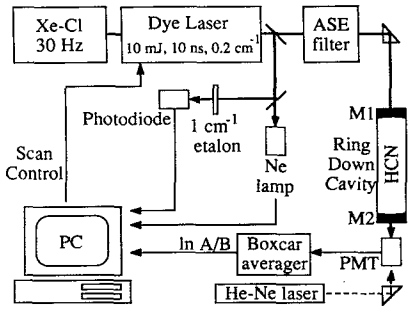

FIG. 1. A schematic of the experimental apparatus.

molecular oxygen. Various schemes for measuring the photon decay time in an optical resonator had been employed earlier, mainly as a means to determine the reflectivity of the dielectric mirrors constituting the resonator itself.[13,14] However, these older applications did not achieve the sensitivity demonstrated by O'Keefe and Deacon.

To measure the decay time of the ring-down signal, O'Keefe used a fast transient digitizer and direct memory access data transfer to a personal computer, with real-time numerical fitting of the digitized profiles. In our setup, we use a two-channel boxcar averager to directly obtain the inverse of the decay time (linearly proportional to the absorption coefficient) as an analog signal which is then digitized and recorded by a personal computer. As we will show below, this simpler and less expensive method gives practically the same sensitivity as O'Keefe's. Two other major differences from O'Keefe are that we do not use transverse mode matching optics and that we filter the amplified spontaneous emission (ASE) from the dye laser beam.

A schematic of the experimental apparatus is shown in Fig. 1. A Xe–Cl excimer pumped dye laser produces pulses of roughly 10 mJ and 10 ns duration at a 30 Hz repetition rate. The instrumental laser line shape is approximately Gaussian with $1/e$ full width of 0.18 cm^{-1}. This was determined by fitting Voigt profiles to etalon peaks measured in transmission, which where characterized by an intrinsic Lorentzian line shape with full width at half-maximum (FWHM) of 0.06 cm^{-1}. The dye laser linewidth can be improved to 0.08 cm^{-1} by using an intracavity etalon, but all measurements reported here are "fast" scans taken at the lower resolution. We choose the HCN pressure ($\sim$100 Torr) to make the line broadening somewhat larger than the 0.18 cm^{-1} instrumental linewidth. This is more than adequate to fully resolve the HCN rotational structure.

A fraction of the laser beam is used to obtain calibration lines from a neon hollow cathode lamp and relative frequency markers from a $\sim$1 cm^{-1} free spectral range etalon. The beam is then filtered through a stimulated Brillouin scattering arrangement, which eliminates the dye laser ASE. Details about this filter will be given after making clear how the ASE can compromise the observed absorption intensity. The beam is then coupled into the RDC high finesse cavity, which is shaped like an absorption cell with the mirrors as windows and is filled with the gaseous HCN sample. The mirrors are oriented with the high reflectivity dielectric coating facing inside the cavity and are mounted on two flanges connected to the sample cell through vacuum tight bellows. These bellows allow fine tilting of the flanges for mirror alignment. For each laser pulse, a small fraction (typically less than 100 ppm) of the intensity traverses the first mirror and then "rings" back and forth inside the cavity. If the pulse duration is shorter than the cavity round-trip time, its leading and trailing edges never overlap inside the RDC and no destructive interference can occur. For this reason, it is not necessary to match the cavity length to the laser wavelength. The intensity decay of the ringing pulse is observed with a low gain phototube (RCA IP28), placed after the output mirror of the RDC. Photomultipliers with high gain are not recommended because the intensity of the signal is quite large and will lead to saturation and nonlinearity.

The requirement that the laser pulse be shorter than the RDC round trip assures that the laser linewidth is larger than the RDC free spectral range. This implies that there is always at least one of the RDC longitudinal modes to transmit part of the laser spectral components. However, even longer pulses may be efficiently coupled into the RDC if they are not Fourier transform limited, which is the most common situation. Another way to impose the same condition is to ask that the laser coherence length, which in general is shorter than the pulse duration, be larger than the RDC round-trip time. An interesting treatment which also accounts for the mode structure of the dye laser has been given by O'Keefe and Deacon.[11] According to this treatment, the relative pulse-to-pulse rms fluctuations of the energy injected in the RDC are given by

$$\frac{W_{\mathrm{rms}}}{\bar{W}} \lesssim \frac{1}{\sqrt{NP}}, \quad \text{in the limit of } P \ll 1, \tag{1}$$

where P is the fraction of RDC modes that fit within the bandwidth of a single laser mode, which is given by the width of the laser modes divided by the RDC free spectral range, and N is the number of active laser cavity modes. Consequently, if NP is larger than 1, the average pulse-to-pulse fluctuations of the energy coupled into the RDC will be relatively small. This explains why, even when the RDC round trip is somewhat shorter than the laser pulse duration, it is still possible to observe a regular ring-down signal. The unstated assumption of this analysis is that couplings of different laser modes into the RDC are statistically independent. This assumption will break down if the ratio of the optical cavity lengths in the laser and the RDC are nearly resonant, since the two sets of modes will be highly correlated.

If the dye ASE is injected into the RDC together with the laser field, it will contribute to a fraction of the observed decay signal. This fraction of the signal is not affected by narrow band absorption features of the sample and produces distortion effects in the absorbance spectrum. Since the ASE is difficult to control, the accuracy and reproducibility of the absolute absorption intensity of the sample is degraded. As such, it was necessary to remove

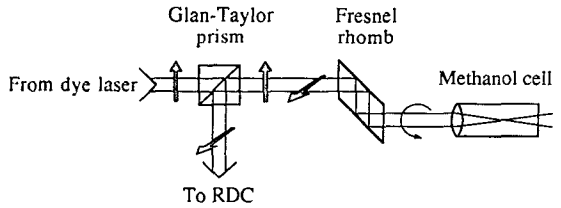

FIG. 2. Brillouin scattering setup for filtering the dye laser ASE. The polarization is represented by the arrows.

this ASE in order to obtain spectra with a reproducible absorption intensity.

The Brillouin scattering setup we use to reject the ASE is shown in Fig. 2. The vertically polarized laser pulse is transmitted by a Glan–Taylor polarizer. A Fresnel rhomb turns the polarization to circular. The pulse is then focused into a liquid (e.g., methanol) so that, at the focal point, the threshold power for stimulated Brillouin scattering is reached and a conjugate pulse is produced. The conjugate pulse counter propagates exactly along the direction of the incoming pulse and has opposite helicity. The phenomenon is described (see Yariv[15]) in terms of a nonlinear interaction of the photon field with the phonon field of the liquid, which transfers energy to a traveling compression wave with half the laser wavelength (whose spectral intensity is dominating over the broadband ASE background). The dependence of the index of refraction on the density of the liquid makes the compression wave act as a diffraction grating whose length is on the order of the beam confocal length Z_0. Therefore, only frequencies in a bandwidth $1/Z_0$ around the center frequency are diffracted backward. Almost all the ASE is transmitted or scattered at other angles. The Fresnel rhomb unfolds the polarization of the conjugated pulse back to linear, but along the horizontal plane, so that the Glan–Taylor polarizer deflects the pulse towards the RDC. The total intensity loss through this filter is about 80% and we do not know which fraction corresponds to ASE. We find the efficiency of the Brillouin process itself to be of the order of 50%, the rest of the losses being due to the optics, which are uncoated.

As a side effect of the ASE filter, the poorly shaped cross section of the dye laser beam is also substantially improved and made more suitable to match the TEM_{00} mode of the resonator. In fact, we do not use any additional optics to improve mode matching to the RDC. Another factor that allows us to observe the decay corresponding to the TEM_{00} mode alone is the very small diameter of our mirrors (4.5 mm). This makes the diffraction losses negligible for the TEM_{00}, but not for the higher order cavity modes. Even if initially excited as a result of imperfect mode matching, these modes decay faster. We often observe oscillations in the signal due to transverse modes beating, but these are usually limited to the very beginning of the exponential decay. In principle, it is desirable to use spatial filtering and telescope optics to match the laser beam waist and size to that of the fundamental transversal mode of the RDC in order to inject the laser energy as efficiently as possible. However, in practice, we found at best a minor improvement in signal/noise when a spatial filter was used.

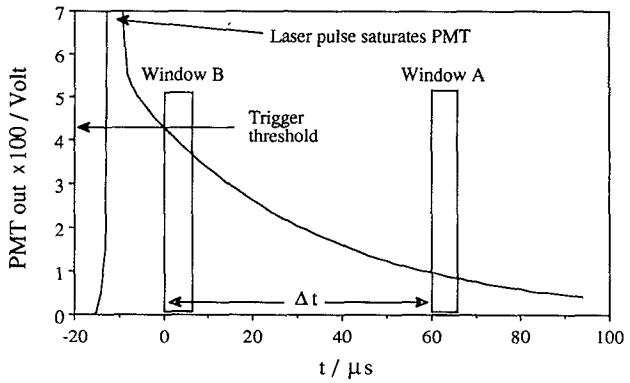

FIG. 3. The PMT ring-down signal as a function of time. Triggering threshold and position of boxcar integration windows are also shown. Δt multiplied by the speed of light gives the effective absorption path length L.

A problem associated with the ASE filter is that since the acoustic wave which acts as a grating travels in the liquid at the speed of sound, the reflected pulse has a Doppler shift equal to $-2\nu v_s/c'$, where ν is the optical frequency, and v_s and c' are the speed of sound and of light in the liquid. Therefore, a small frequency shift is introduced (of the order of $-0.2\ \mathrm{cm}^{-1}$) with respect to the calibration lines produced by the neon hollow cathode lamp which is placed before the filter. We corrected for this shift by using a constant speed of sound and a constant index of refraction (1203 m/s and 1.3288 for methanol).[16] We also measured the shifts at several frequencies by comparing calibration line centers with respect to the etalon peaks in scans taken with the neon lamp placed before and after the ASE filter. We found a reasonable agreement with the calculated shifts, with differences of the order of $0.02\ \mathrm{cm}^{-1}$, which is the uncertainty in the line centers determination.

A Tektronix AM502 is used to amplify the photomultiplier tube (PMT) output roughly 100 times and bring it in the range of a few volts of peak intensity. The amplifier bandpass is adjusted to smooth out the structure in the signal which corresponds to the pulse round trip inside the cavity. A boxcar averager (Princeton Applied Research, model 162, with two gated integrator channels model 165) is then triggered to the signal itself, at a point with an average delay from the laser pulse equal to a few times τ. The initial signal intensity shows pulse to pulse fluctuations of the order of 50%, and this scheme of triggering always probes the same intensity range of each decay. This is especially desirable in order to minimize the effect of small PMT nonlinearity.

The two boxcar channels (A and B) are set to integrate and average the decay inside two time windows. The window width ($\sim 5\ \mu s$) and the integration time constant ($10\ \mu s$) are the same for A and B. Window B opens at the trigger point, while window A opens after a delay Δt, as shown in Fig. 3. Our boxcar has a built-in analog output function $\log(A/B)$, which turns out to give

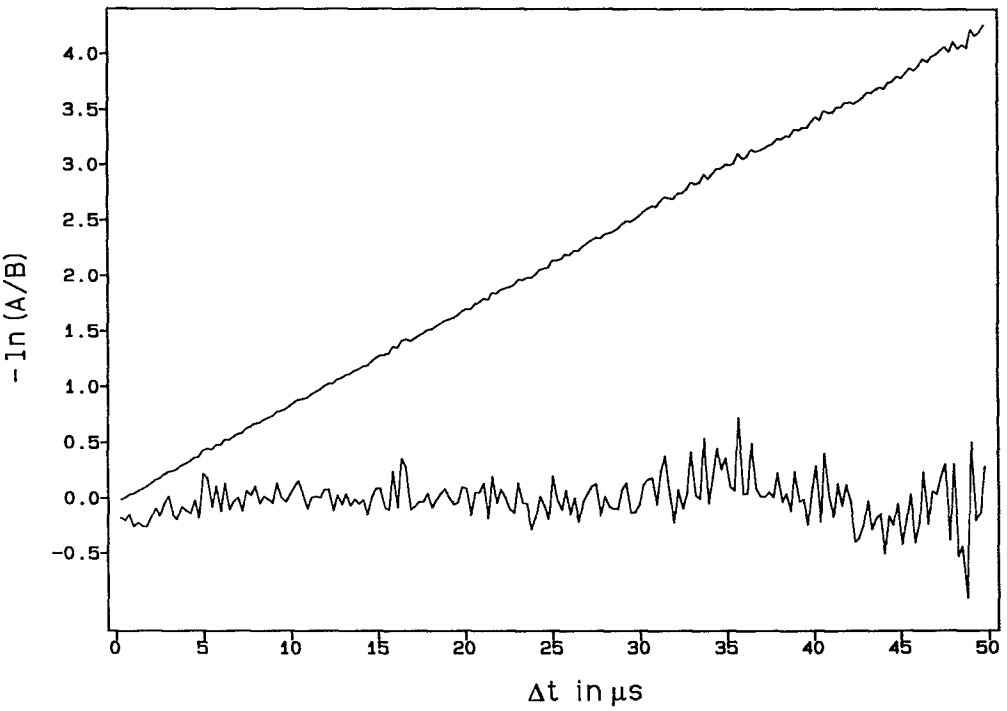

FIG. 4. The RDC boxcar output when the window delay Δt is linearly ramped from 0 to 50 μs. The decay time in this case is $\tau = 12$ μs and the effective path length that optimizes the signal to noise is $L \simeq 7$ km. The residuals of a linear fit, amplified ten times, are also plotted to display the noise level.

$S = -\Delta t/\tau - \alpha c \Delta t$ (see the next section), where α is the sample absorbance per unit length experienced by the ringing pulse inside the RDC and c is the speed of light. The RDC decay time constant is given by $\tau \simeq l/c(1-\mathscr{R})$, where l is the length of the cell and $\mathscr{R}$ is the reflectivity of the mirrors. The optimal window delay Δt is on the order of 2τ, and the corresponding quantity $L = c\Delta t$ is the effective absorption path length, on which the high sensitivity of this technique depends. Values of L on the order of tens of kilometers can be easily obtained.

The suppression of PMT nonlinear response obtained by triggering on the decay signal itself may be understood in the following simple way: If the PMT response depends on the intensity of the signal itself, we may write G_A and G_B as the gain factors corresponding to the intensity level in windows A and B, respectively. This is clearly a good approximation only if the PMT gain does not change too rapidly with the intensity. When $\log(A/B)$ is evaluated, these gain factors give a baseline shift in the spectrum equal to $\log(G_A/G_B)$. This is a constant only if the signal intensities in window A and in window B are always approximately the same. If we were using a constant delay triggering scheme, this baseline shift would vary from shot to shot and would become a source of noise.

To test if the observed RDC decay is really exponential, we choose a laser frequency not resonant with any absorption line ($\alpha \sim 0$) and record the boxcar output as a function of Δt. This is done by linearly ramping in time the delay between the integration windows. If the decay is indeed a pure exponential, then we expect to see a straight line $-\Delta t/\tau$, as shown in Fig. 4. This test also conveys information on the signal to noise ratio as a function of Δt. It can be seen from Fig. 4 that the noise level starts to increase rapidly approximately for $\Delta t > 2\tau$. This is consistent with a noise level proportional to the inverse square root of the ring-down signal, suggesting that statistical shot noise is dominating. Since the sensitivity increases linearly with Δt, the maximum signal to noise ratio is in general achieved for a delay value equal to 2τ.

We use a He–Ne laser beam to make the RDC alignment reasonably simple. If the working range of the RDC mirrors does not include the He–Ne wavelength, then it is convenient to keep a He–Ne laser aligned to the cavity axis so that the beam transmitted through the RDC can be seen together with a few reflected ones. This makes alignment of the mirrors straightforward. Two irises, placed close to the RDC input mirror and to the output of the Brillouin filter (50 cm away), are aligned to the He–Ne trace and are very convenient for quick alignment of the dye laser beam to the RDC axis. After these adjustments to the mirrors and the dye laser beam, the PMT output can be monitored with an oscilloscope and small corrections to the mirrors may be needed to optimize the decay time and the quality of the signal. Having a He–Ne laser permanently positioned is especially useful when the RDC needs to be realigned frequently. This happens, e.g., when changing the sample pressure or the scanning range.

To cover the spectral range of each HCN overtone, we used three pairs of high reflectivity mirrors. For the fifth overtone (006 and 105 bands), the mirrors (covering the range 520–640 nm) were kindly provided by Professor J. C. Bergquist at NIST, Boulder (Colorado). For the sixth

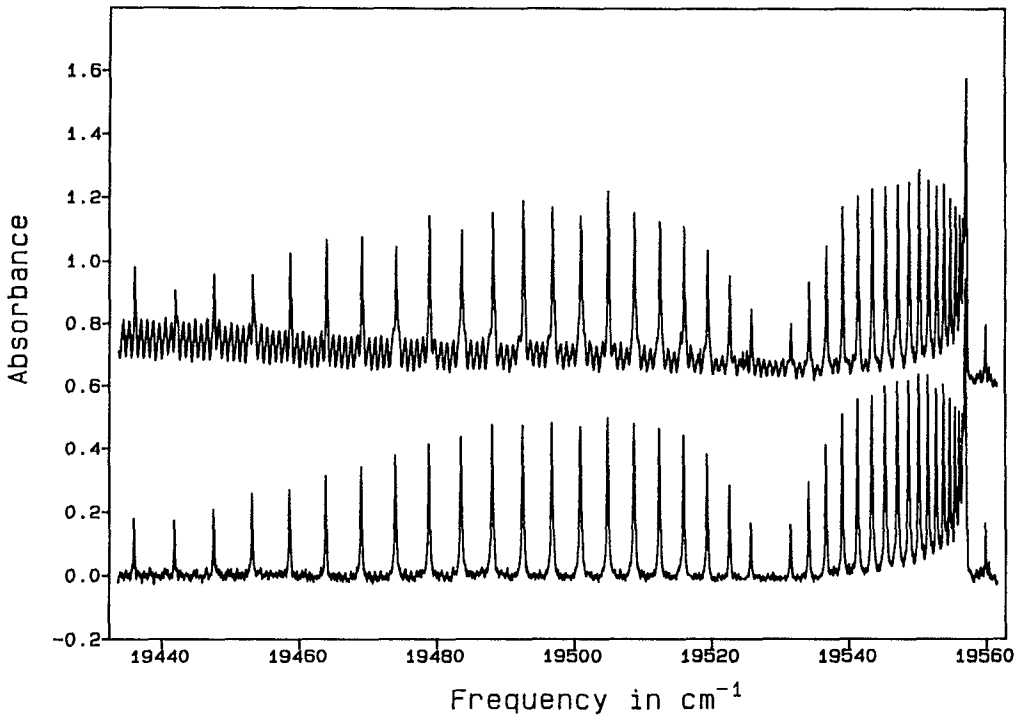

FIG. 5. A spectrum of the 205 HCN overtone band (100 Torr, $\Delta t=80$ μs, and $L=24$ km) is shown before and after baseline correction. The baseline etaloning is very regular and has been removed completely by subtracting a sinusoidal function of linearly decreasing amplitude. The peak before the bandhead is an unassigned water overtone line (showing that in this scan we had some problems with the sample purity).

and seventh overtones, we used two sets of mirrors (good in the ranges 450–520 and 430–490 nm) acquired from PMS Electro-Optics.[17] Unfortunately, these mirrors did not allow us to cover the region where the 008 band is expected to be (420 nm).

The cell length l is a compromise between opposing requirements. Since the RDC decay time is dominated by the mirror losses and transmittivity, the cavity length should be maximized. On the other hand, the maximum length is determined by the finite length of our optical table (3 m) and by the request that the cavity be stable with respect to the beam size. According to the theory of stable resonators,[15] in the case of two mirrors with the same radius of curvature r, the transverse modes of the resonator have a finite size if the cavity length is less than $2r$ (their size diverges for this value). The 520–640 and 430–490 nm mirrors had a large curvature radius which allowed us to use the full length of the table. In the 450–520 nm region, only 1 m curvature mirrors were available, with a coated reflective surface of 4.5 mm diameter, for which we calculated that the diffraction losses of the TEM_{00} mode are smaller than the mirror transmittivity if the cell is shorter than 1.8 m. In this case, we actually used a 1.3 m long RDC. The mechanical alignment of the mirrors is most forgiving when the RDC is close to confocal ($l=r$) and becomes extremely critical when either the concentric ($l=2r$) or planar ($l \ll r$) limits are approached.

It should be noted that, at wavelengths shorter than ~450 nm, the Rayleigh scattering from the gas sample starts to contribute significantly (it increases with the fourth power of the frequency) to the losses of the cavity. For example, with a 1.3 m long RDC, at 450 nm, we measured a cavity decay time of 23 μs when the cell was evacuated, and 16 μs when the cell was filled with 1 atm of air. With 100 Torr of HCN, the effect of the Rayleigh scattering was still negligible.

In some of our spectra, the baseline is affected by a regular undulation whose free spectral range turns out to be consistent with the mirror's thickness. In the next section, we show that even if the uncoated surfaces of the mirrors have a much smaller reflectivity than the coated ones, the etaloning effect may be quite large. A possible solution is to use antireflection coating on the back of the mirrors, but we found it quite simple and effective to subtract the undulation by manually fitting a sinusoidal function with appropriate period, phase, and amplitude. In Fig. 5 is an example showing how well this baseline correction has worked.

As stated before, the fact that the maximum signal to noise ratio is found for $\Delta t \simeq 2\tau$ suggests that the noise level is dominated by statistical shot noise. Simple theoretical details are given in the next section, but first we want to show that the sensitivity we achieve is indeed shot noise limited. The shot noise at the output of the boxcar (recorded as the signal S) in the limit of $t_w \ll \tau$ has an expected standard deviation $\sigma_S \simeq 1.44S/\sqrt{I_0 t_w}$, where $t_w \simeq 5$ μs is the boxcar integration window duration and τ is roughly equal to 30 μs. I_0 is the initial electron current at the PMT photocathode in units of electrons per second. To estimate

this current, we can start from the fact that the boxcar is triggered by the decay signal itself at a threshold of 5 V. Since the PMT output is amplified 100 times and the PMT impedance is 50 Ω, the PMT output current at the beginning of the portion of decay signal considered is ~ 1 mA. We measured the current gain of our PMT at the typical supply voltage of 900 V and we found that it is of the order of 1×10^5. Therefore, the photoelectron current is $I_0\simeq 10$ nA, which is 6×10^{10} electrons per second. Using this result and the fact that $S=-\Delta t/\tau\simeq 2$, the shot noise standard deviation turns out to be 5×10^{-3} for a single laser shot. The number of laser shots that is averaged for each data point is ~ 10, which decreases the noise by a factor $\sqrt{10}$. The result (2×10^{-3} absorbance units) is almost exactly equal to the standard deviation of the noise level in our spectra. Later on, we will give as a typical noise level on S the canonical $2\sigma_S$ value equal to 0.005.

A last technical note about the mirror performance—as was pointed out to us recently,[17] if the RDC is evacuated too quickly before filling it with the sample, water vapor condenses on the mirror surfaces and leaves deposits which may degrade the reflectivity dramatically. In fact, by pumping on our RDC more slowly than we used to in the past, we observed a fourfold increase of the ring-down time (using mirrors in the 550 nm range, τ increased from ~ 30 to 120 μs).

III. THEORY

After the first pass through the RDC, the laser pulse initial intensity I_{in} is attenuated to $I_0=\mathscr{T}^2\exp(-\alpha l)I_{in}$, where $\mathscr{T}$ is the mirror transmittivity, α is the frequency dependent absorption coefficient of the gas sample inside the cell, and l is the cell length. For each subsequent round trip, the intensity decreases by an additional factor $\mathscr{R}^2\exp(-2\alpha l)$, where $\mathscr{R}$ is the reflectivity of the mirrors. Therefore, after n round trips, the pulse intensity at the PMT is $I_n=[\mathscr{R}\exp(-\alpha l)]^{2n}I_0$. Diffraction losses and Rayleigh scattering by the gas can be included in the mirror losses $\mathscr{L}$, which are linked to the transmittivity and the reflectivity by the conservation of energy $\mathscr{L}+\mathscr{T}+\mathscr{R}=1$. For very high quality dielectric mirrors $\mathscr{L}\simeq\mathscr{T}<100$ ppm. Therefore

$$I_n=I_0\exp[2n(\ln\mathscr{R}-\alpha l)]\simeq I_0\exp[-2n(\mathscr{T}+\mathscr{L}+\alpha l)]. \tag{2}$$

Since the PMT output signal is filtered with a time constant that gives only the intensity envelope of the pulse train, we can change from the discrete variable n to the continuous time variable $t=2nl/c$,

$$I(t)=I_0\exp\left(-\frac{t}{\tau}-c\alpha t\right), \tag{3}$$

where we introduced the empty cavity decay time $\tau=l/c(\mathscr{T}+\mathscr{L})$.

Boxcar channel A integrates the signal over the time window (t_A,t_A+t_w). Neglecting the boxcar integration time constant, this integral is

$$\begin{aligned}\mathscr{A}&=\int_{t_A}^{t_A+t_w}I_0\exp\left(\frac{-t}{\tau'}\right)dt\\&=I_0\exp\left(\frac{-t_A}{\tau'}\right)[1-\exp(-t_w/\tau')]\tau'\\&=I(t_A)[1-\exp(-t_w/\tau')]\tau'\end{aligned} \tag{4}$$

where $1/\tau'=1/\tau+c\alpha$. Since we set the same window width t_w for both channels A and B, the boxcar output is

$$S=\ln(\mathscr{A}/\mathscr{B})=\ln[I(t_A)/I(t_B)]=-\frac{\Delta t}{\tau}-L\alpha, \tag{5}$$

where Δt is the delay between window A and B, and $L=c\Delta t$ is the "effective path length" over which the absorption coefficient α is measured. If the window delay is kept constant, the term $\Delta t/\tau$ can be considered as a slowly varying baseline. The signal S is recorded while the laser is tuned at a conveniently slow rate and can be directly converted to units of fractional absorption per unit length and unit pressure by using the effective absorption path length L and the gas pressure in the cavity. We already observed in the Experimental section that the best signal to noise is achieved approximately when $\Delta t=2\tau$. By setting the window delay to this optimal value, one fixes the effective path length to $2c\tau$. In theory, for mirrors with transmittivity better than 100 ppm and comparable losses, one should obtain a decay time longer than 100 μs for a 3 m long cell. Recently in our laboratory, we have observed a decay time value as good as $\tau\simeq 120$ μs, for which the optimal Δt corresponds to $L=72$ km. However, at the time the reported data were taken, the best values that we could obtain were $\tau=40$ μs and $L=24$ km.

The experimental noise level of the signal S is $2\sigma_S\simeq 0.005$. Incidentally, if it is considered that this noise is due mostly to the integration over window A (where the decay signal is much weaker), then this figure means that we are able to observe a 1% variation in $\mathscr{A}$,

$$2\sigma_S=\left|\frac{\partial S}{\partial\mathscr{A}}\right|2\sigma_{\mathscr{A}}=\frac{2\sigma_{\mathscr{A}}}{\mathscr{A}}=0.5\%. \tag{6}$$

The sensitivity limit is obtained dividing σ_S by the effective path length

$$\begin{aligned}2\sigma_\alpha&\simeq\frac{0.005}{72\text{ km}}\simeq 7\times10^{-10}/\text{cm}\times 300\text{ cm/round trip}\\&=2\times10^{-7}/\text{round trip},\end{aligned} \tag{7}$$

i.e., 0.2 ppm per round trip.

At this point, we want to show that the etaloning between the coated and uncoated surfaces of each mirror can produce a sizeable baseline undulation as the laser frequency is tuned. We have observed this effect in several of our spectra, and the strongest indication that it is etaloning between the mirror surfaces is that its free spectral range is consistent with the thickness of the mirrors.

In dealing with interference effects, we have to consider the field amplitude of the laser pulse rather than the

intensity. For simplicity, we will consider an empty cell for which $\alpha=0$. The electric field E_r, reflected inside the RDC by the two surfaces of one of the mirrors, can be written in terms of the incident field E_i as $E_r=(r_c+r_u t_c^2 \exp i\phi)E_i$ where $r_c=\sqrt{\mathscr{R}}$ and $r_u\simeq 0.2$ are the field reflectivities of the coated and uncoated surfaces, $t_c=\sqrt{\mathscr{T}}$ is the field transmittivity of the coated surface, which is related to its reflectivity by $t_c^2+r_c^2=\mathscr{T}+\mathscr{R}=1-\mathscr{L}$. The phase shift for the portion of the pulse which is transmitted by the coated surface and then partially reflected back by the uncoated one is $\phi=4\pi\nu d+\pi$, since it travels twice the optical mirror thickness d. Finally, ν is the laser frequency in wave numbers.

After n round trips, $E_n=(r_c+r_u\mathscr{T}\exp i\phi)^{2n}E_0$, which is accurate except for an irrelevant phase factor. Following the same argument as before, the boxcar output is

$$S=\ln\frac{|E(t_A)|^2}{|E(t_B)|^2}=2(n_A-n_B)\ln(r_c^2+2r_u r_c\mathscr{T}\cos\phi+\mathscr{T}^2 r_u^2)$$

$$\simeq\frac{c\Delta t}{l}\ln(1-\mathscr{T}-\mathscr{L}+2r_u\mathscr{T}\cos\phi)$$

$$\simeq-\frac{\Delta t}{\tau}\left[1-\frac{2\mathscr{T}}{\mathscr{T}+\mathscr{L}}r_u\cos(4\pi\nu d)\right] \tag{8}$$

Since $\Delta t=2\tau$ and $\mathscr{T}\lesssim\mathscr{L}$, the peak-to-peak amplitude of the baseline undulation turns out to be smaller than $4r_u=0.8$. The experimental baseline etaloning was in all cases smaller than 0.1. However, we have not considered a factor that should diminish the etalonings amplitude appreciably. In fact, the fraction of the pulse reflected by the mirror uncoated surface suffers big diffraction losses because this surface is flat, and thus, does not match the phase front of the reflection off the curved high reflective surface of the optic. As counterintuitive as it may be, this upper limit estimate shows that the etaloning due to the uncoated mirror surfaces can indeed be quite large.

The next issue is to establish the theoretical limit of the sensitivity of the RDC apparatus. This limit is obtained by assuming shot noise as the dominant noise factor. Shot noise is associated with fluctuations in the intensity of the signal due to the quantization of the signal carriers. The fluctuations are proportional to the square root of the number of carriers. As such, the largest fractional noise is produced where the current of carriers is smallest. In the case of the RDC, this occurs at the level of the photoelectrons emitted by the PMT photocathode. The shot noise level is then proportional to the square root of the current of these photoelectrons, which we write as $I(t)=I_0\exp(-t/\tau)$, where from now on τ is the effective RDC decay time including any sample absorption. In the following, the noise associated with a variable v will be denoted by σ_v.

Below we derive the theoretical lower limit of the noise level in four signal processing schemes that extract the decay time from the RDC exponential decay signal. These schemes include the one we used and the one employed by O'Keefe.[11] Of the other two, one should be considered as a limiting case of theoretical interest and the last one appears to be very easy to implement and should give the best performance. However, one of the outcomes of the following arguments is that the shot noise limit in different signal processing methods is not significantly different.

First, we deal with the simpler boxcar scheme. We want to find the fractional noise associated with the decay time constant τ, derived as described above by integrating the decay signal in window A and B, with A delayed by Δt with respect to B. The boxcar output is $S=\ln(\mathscr{A}/\mathscr{B})=-\Delta t/\tau$, so that $\sigma_\tau/\tau=\sigma_S/S$ and $\sigma_S^2=(\partial S/\partial\mathscr{A})^2\sigma_{\mathscr{A}}^2+(\partial S/\partial\mathscr{B})^2\sigma_{\mathscr{B}}^2=(\sigma_{\mathscr{A}}/\mathscr{A})^2+(\sigma_{\mathscr{B}}/\mathscr{B})^2$. The noise level of $\mathscr{A}$ (and analogously for $\mathscr{B}$) can be written as

$$\sigma_{\mathscr{A}}^2=\int_{t_A}^{t_A+t_w}\left[\frac{\partial\mathscr{A}}{\partial I(t)}\right]^2\sigma_I^2(t)dt=\int_{t_A}^{t_A+t_w}\sigma_I^2(t)dt, \tag{9}$$

which is simply the generalized rule for the propagation of errors. The last equality is a consequence of the definition of $\mathscr{A}$, which implies that $\partial\mathscr{A}/\partial I(t)$ is identically one. Now let us choose the boxcar trigger as the time origin, so that we have $t_B=0$ and $t_A=\Delta t$. Solving the integrals for $\sigma_{\mathscr{A}}$ and for $\sigma_{\mathscr{B}}$, one gets

$$\sigma_S^2(\Delta t)=\frac{1}{I_0\tau}\frac{1}{1-\exp(-t_w/\tau)}[1+\exp(\Delta t/\tau)]. \tag{10}$$

Now we can choose Δt to minimize the fractional noise of τ,

$$\frac{\sigma_\tau}{\tau}=\frac{\sigma_S}{S}=\frac{1}{\sqrt{I_0\tau}}\frac{1}{\sqrt{1-\exp(-t_w/\tau)}}\frac{\sqrt{1+\exp x}}{x},$$

$$x=\frac{\Delta t}{\tau}. \tag{11}$$

As anticipated in the experimental section, the minimum occurs close to 2τ, and more precisely for $\Delta t_{\min}\simeq 2.22\tau$, so that

$$\left.\frac{\sigma_\tau}{\tau}\right|_{\min}=\frac{1.44}{\sqrt{I_0\tau}}\frac{1}{\sqrt{1-\exp(-t_w/\tau)}}\gtrsim\frac{1.44}{\sqrt{I_0\tau}},\quad \text{if } t_w\gtrsim\tau. \tag{12}$$

In fact, the function $f(t_w/\tau)=\sqrt{1-\exp(-t_w/\tau)}$ goes to the limiting value 1 very rapidly $f(1)=0.795$, $f(2)=0.930$, etc. When we took our measurements, we used a relatively small value of 4.5 μs for t_w. Together with the 40 μs value for τ, we obtain $\sigma_\tau/\tau|_{\min}\simeq 4.4/\sqrt{I_0\tau}$, which is only a factor of 3 worse than the limiting best value.

We follow a similar analysis for O'Keefe's method. Here, the decay signal is digitized in a time interval $[0,T]$ and then its logarithm is least squares fitted to a straight line to extract the slope $a=-1/\tau$. In the following, instead of summing over data points, it will be convenient to use integrals. The signal is in this case $S(t)=\ln I(t)=\ln I_0-t/\tau$ with a noise level $\sigma_S^2(t)=(\partial S/\partial I)^2\sigma_I^2(t)=1/I(t)$. The least-squares fit involves minimizing

$$F(a,b)=\int_0^T[S(t)-at-b]^2\,dt \tag{13}$$

with respect to a and b, from which

$$a=\frac{12}{T^3}\int_0^T tS(t)dt-\frac{6}{T^2}\int_0^T S(t)dt \rightarrow \frac{\partial a}{\partial S(t)}=\frac{12}{T^3}t-\frac{b}{T^2}. \tag{14}$$

This allows us to calculate the noise level of a,

$$\sigma_a^2(T)=\int_0^T\left[\frac{\partial a}{\partial S(t)}\right]^2 a_S^2(t)dt$$

$$=\frac{36}{I_0\tau^3}\frac{(x^2-4x+8)e^x-x^2-4x-8}{x^6},$$

$$x=\frac{T}{\tau}, \tag{15}$$

which should be minimized to find the optimal experimental conditions

$$T_{\min}\simeq 3.52\tau \rightarrow \left.\frac{\sigma_\tau}{\tau}\right|_{\min}=\left.\frac{\sigma_a}{a}\right|_{\min}=\frac{1.84}{\sqrt{I_0\tau}}. \tag{16}$$

This is just slightly worse than the previous result [Eq. (12)]. It might seem puzzling that $T_{\min}$ is actually finite. This implies that one should record and fit only a finite portion of the ring-down decay signal. The problem is that a nonweighted least-squares fit is used here, and the shot noise on the logarithm of the ring-down signal increases exponentially with T. If all times are equally weighted, then the fit becomes more and more affected by the shot noise as T is increased beyond $T_{\min}$.

What happens if the fit to $S(t)$ is weighted with the inverse square of the shot noise? We find that in this case, the minimum noise occurs for $T\rightarrow\infty$,

$$\frac{\sigma_\tau}{\tau}=\frac{1}{\sqrt{I_0\tau}}. \tag{17}$$

This probably represents the best shot noise limit that can be obtained in any signal processing scheme.

Finally, a fourth case is quite interesting because it could be easily implemented by using some analog electronics (integrators, ramp generators, and multipliers) plus an averager. The idea is to calculate

$$\tau=\int_0^\infty tI(t)dt \Big/ \int_0^\infty I(t)dt. \tag{18}$$

It turns out that this last simple scheme has the same shot noise limit as the weighted least-squares fitting method [Eq. (17)]. A disadvantage is that it does not allow a simple experimental test for the pure exponential character of the decay, as can be done in the case of the boxcar scheme by ramping the window delay.

Noting that $I_0=N_0Q\mathcal{T}^2(c/2l)$, we can relate Eq. (17) to experimental parameters, indicating with N_0 the number of photons striking the input mirror of the RDC and with Q the quantum efficiency of the detector. For the noise equivalent absorbance α, we have

$$\sigma_\alpha=\frac{1}{c\tau}\frac{\sigma_\tau}{\tau}=\left(\frac{1}{l\sqrt{QN_0}}\right)\sqrt{\frac{2(\mathcal{T}+\mathcal{L})^3}{\mathcal{T}^3}}$$

$$\simeq\left(\frac{1}{l\sqrt{QN_0}}\right)4\sqrt{\mathcal{T}},\quad \text{if } \mathcal{T}\simeq\mathcal{L}. \tag{19}$$

The term in brackets is the noise-equivalent α expected for a single pass with a shot noise limited laser source. Even in this ideal case, the RDC improves sensitivity by a factor of $1/4\sqrt{\mathcal{T}}$. In practice, the gain is much higher because a pulsed laser system is unlikely to be shot noise limited.

As a measure of what is possible with the RDC, we would like to point out that Rempe *et al.*[18] recently reported mirrors with total losses $\mathcal{T}+\mathcal{L}\sim 10^{-6}$ (measured at 850 nm with a 4 mm long RDC). Combining this with $QN_0\sim 10^{15}$, corresponding to a few milliJoules pulse, and $l=2$ m, σ_α is calculated to be $\sim 1\times 10^{-12}$/cm on a single laser pulse, which we believe to be orders of magnitude better than has ever been realized in any absorption based detection method.

To obtain accurate absolute absorption measurements, it is very important that any offset to the ring-down signal be accurately removed. In O'Keefe's scheme, the digitizer is pretriggered and a portion of the baseline just before the signal is sampled and then numerically subtracted before applying the logarithm. In our scheme, the baseline is zeroed by blinding the PMT and tuning the boxcar input offset of each channel until the corresponding integral is zero. To ensure that subsequent baseline drifts give a negligible contribution, we choose a relatively small t_w, so that the signal in the integration window is always much larger than the baseline. In the triggering scheme we use, a t_w smaller than τ makes the suppression of PMT nonlinearity more effective.

IV. MEASUREMENTS AND DATA ANALYSIS

Typical experimental conditions have already been outlined in a previous section. Since none of the recorded HCN overtone bands is affected by perturbations, the grating-mode resolution (0.2 cm^{-1}) of the dye laser system is sufficient to completely resolve the rotational structure of the spectra, which is dominated by self-broadening at a pressure of 100 Torr.

We scan over HCN overtone bands using 0.005 cm^{-1} steps and average for 0.5 s the RDC boxcar output with a computer, using a boxcar time constant of 0.1 s. At the same time, the signals from the neon calibration lamp and the external reference etalon, processed by another boxcar, are also recorded. The reference etalon transmission peaks are used for frequency linearization of the spectra. We determined the free spectral range of our etalon to be 0.992 71 cm^{-1} by reference to neon calibration lines in a scan over the interval 540–570 nm. Since this is an air spaced etalon, the free spectral range is practically the same for all the spectra we have recorded. After linearizing, the neon calibration lines give an absolute frequency calibration good to ± 0.02 cm^{-1}.

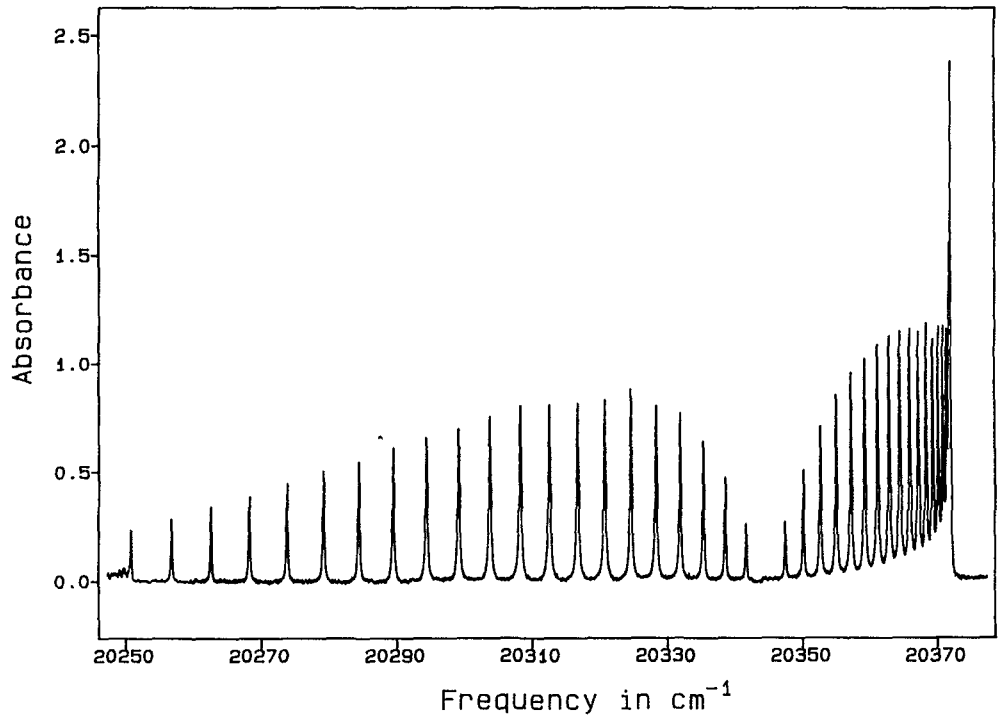

FIG. 6. The spectrum of the 106 overtone of HCN (100 Torr, $\Delta t=80$ μs, and $L=24$ km). Near the last displayed line of the P branch is the beginning of the hot band, which is shown in Fig. 8.

Using the A/D digitalization factor, the spectra are converted to absolute absorbance units. The baseline is then adjusted by subtracting a polynomial interpolating function fitted to free baseline sections. Baseline variations in RDC spectroscopy are caused principally by the slow dependence of the mirror's reflectivity on the laser frequency. In some of the spectra, a regular etaloning affects the baseline. This defect could be removed by subtraction of a manually fitted sinusoidal function. In Fig. 5 is an example of a spectrum before and after correcting the baseline. The baseline etaloning in this example is one of the worst cases we had to deal with. In Fig. 6, the "best spectrum" is shown, where it can be noticed that the noise level increases appreciably at the absorption peaks (see also the residuals of the fit in Fig. 7). In this scan, the delay between the integration windows had been set to optimize the signal to noise ratio at the baseline (according to the condition $\Delta t=2\tau$). However, this delay is too long when τ decreases by as much as 30% in correspondence with an absorption peak. To achieve a more homogeneous noise level, other measurements of strong bands have been taken setting a delay Δt smaller than 2τ.

The line positions and the integrated intensities, as well as the Lorentzian half-widths, are obtained from a nonlinear least-squares fit of the spectrum. The model used in this fit is given by a sum of Lorentzian functions convoluted with a single normalized Gaussian profile. The Gaussian width is given by the sum in quadrature of the laser width (0.18 cm^{-1} $1/e$ full width) and of the calculated HCN Doppler broadening. As an example, the result of the fit to the R branch of the 106 band is shown in Fig. 7.

The line positions of each band are then fitted to a rotational model including the centrifugal distortion parameter ΔD. The ground state constants B_0 and D_0 are constrained to the very accurate microwave-IR values ($B_{000}=1.478\,221\,834$, $D_{000}=2.9099\times10^{-6}$, $B_{010}=1.481\,773$, and $D_{010}=2.9729\times10^{-6}$).[19]

The joint accuracy of the frequency calibration procedure and of the Brillouin shift correction (discussed before) is of the order of 0.03 cm^{-1}. This is much larger than the statistical standard deviation of the fitted band origins (usually 0.005 cm^{-1}, with the exception of the very weak $117\leftarrow010$ hot band, whose standard deviation is 0.02 cm^{-1}). In Table I, we list the values of the band origins and compare them to the outcomes of some theoretical calculations. The results by Carter, Handy, and Mills[20] using an empirical potential surface[9] adjusted to all HCN data up to those recorded by Yang *et al.*[8] show an impressive agreement with our data. The average deviation is somewhat larger than 1 cm^{-1}. From an adjusted Murrell–Carter–Halonen potential are the results of Gazdy and Bowman[21] in column four of the same table. The *ab initio* values by Botschwina[22] are particularly impressive too, especially if one considers that they are based on a simplified two-dimensional model of the HCN molecule. In the last column of Table I are the frequencies calculated with the anharmonic expansion by Smith *et al.*[6]

Table II lists the fitted rotational parameters together with the calculated ones. Errors on ΔB and ΔD are given as two standard deviations. In most cases, it is clear that the uncertainty in the line positions is too large to obtain significant ΔD values. The values of ΔB calculated by

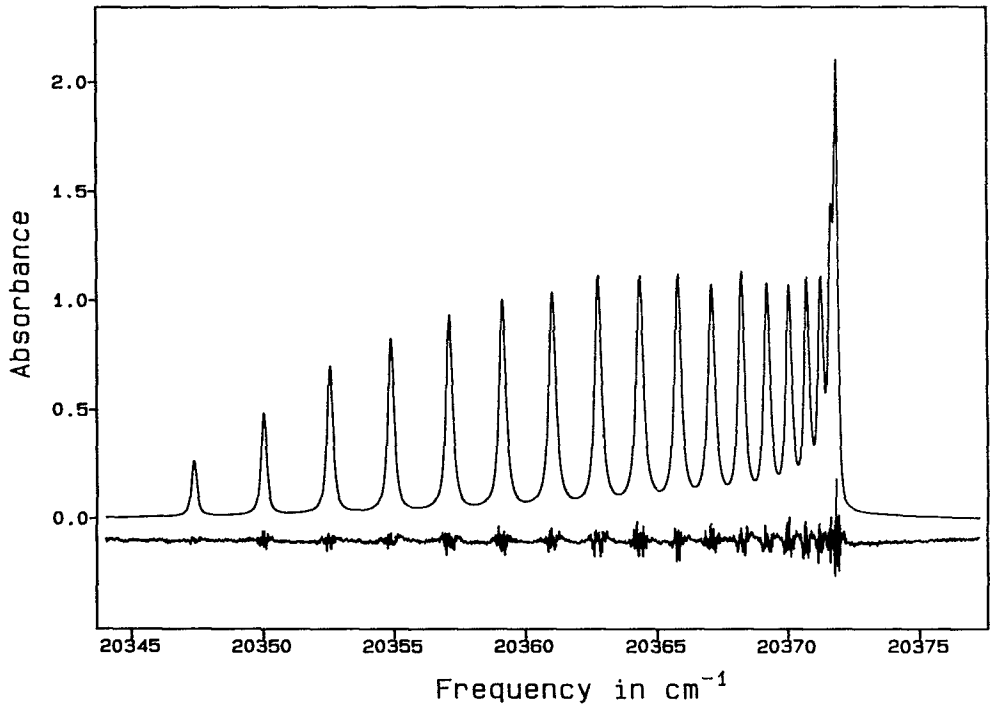

FIG. 7. The result of the fit to the 106 bandhead with a sum of independent Lorentzian functions. The residuals are also shown, shifted negatively for clarity. See the text for a comment about the increasing noise level at the peaks.

Carter *et al.*[20] with the same potential as before appear to underestimate the experimental data, and the deviation systematically increases at higher energies. On the other hand, those that we have calculated using the anharmonic expansion by Smith *et al.*[6] perform much better.

We tested for the presence of perturbations in the rotational structure of these overtones in the following way: For each band, we compared the standard deviation of the combination differences of the data from the expected values (which depend only on the ground state rotational constants) against the standard deviation of the rotational fit. We always found comparable values, implying that no observable perturbations are present.

For each line, the integrated line intensity (LI) has been converted to band intensity (BI) according to the relation:

$$\mathrm{LI}(J,T)=\mathrm{BI}\times\mathrm{HL}(J)\times P(T)\times F, \tag{20}$$

where HL is the Hönl–London factor, as a function of the angular momentum J; P is the starting energy level thermal population as a function of the temperature T; and F is the isotopic fraction. All that is needed to calculate these factors for HCN is reviewed in Ref. 6. By using the HCN RDC pressure and the effective absorption path length $L=c\Delta t$, these BIs can be expressed easily in units of

TABLE I. A comparison of the experimental band origins with calculations by Carter, Handy, and Mills (Refs. 9 and 20) by Gazdy and Bowman (Ref. 21) and by Botschwina (Ref. 22). The experimental error bar is dominated by the inaccuracy in the absolute frequency calibration. The values by Carter *et al.* are based on the same potential used for the rotational constants of Table II. In the last column are reported frequencies that we calculated using the anharmonic expansion fitted by Smith *et al.* in Ref. 6.

Transition	Expt. ($\pm$0.03 cm^{-1})	C.H.M.	G.B.	Botschwina	Smith
105←000	17 550.421	17 549.59	17 557.0	17 526.7	17 559
006←000	18 377.031	18 376.47	18 375.1	18 348.8	18 377
205←000	19 528.575	19 527.34	19 538.5	19 501.5	19 547
116←010	20 222.275	20 222.27	...	...	20 242
106←000	20 344.510	20 342.10	20 353.2	20 309.8	20 361
007←000	21 116.314	21 115.25	21 122.8	21 078.5	21 115
305←000	21 486.774	21 485.42	21 500.4	21 456.6	21 514
206←000	22 292.022	22 288.96	22 312.8	22 250.9	22 325
117←010	22 903.488	22 905.22	...	...	22 935
107←000	23 047.106	23 043.37	23 080.0	23 000.7	23 074

TABLE II. Rotational parameters of the observed HCN overtone bands. Error bars for the experimental values are two standard deviations of the fit. Ground state constants were constrained to the microwave-IR values ($B_{000}=1.478\,221\,834$, $D_{000}=2.9099\times10^{-6}$, $B_{010}=1.481\,773$, $D_{010}=2.9729\times10^{-6}$) (Ref. 19). In the third column are ΔB's calculated by Carter, Handy, and Mills (Ref. 20) using a potential surface (Ref. 9) fitted to all previous HCN data including SEP spectra by Yang *et al.* (Ref. 8). In the fourth column are values calculated by us employing the anharmonic expansion by Smith *et al.* (Ref. 6).

Transition	ΔB (Expt.) ($\times10^3$ cm^{-1})	ΔB (C.H.M.) ($\times10^3$ cm^{-1})	ΔB (Smith) ($\times10^3$ cm^{-1})	ΔD (Expt.) ($\times10^6$ cm^{-1})
105←000	−64.2 ±0.3	−64.2	−64.2	···
006←000	−67.1 ±0.4	−67.6	−67.1	···
205←000	−72.70±0.03	−72.7	−73.2	0.10±0.05
116←010	−74.4 ±0.4	···	−71.2	···
106←000	−75.69±0.06	−75.7	−75.9	−0.13±0.24
007←000	−79.31±0.10	−77.2	−79.4	0.08±0.24
305←000	−81.96±0.18	−72.7	−82.3	−1.5 ±0.8
206←000	−84.00±0.08	−80.7	−84.7	0.19±0.16
117←010	−85.8 ±0.8	···	−86.6	···
107←000	−87.57±0.06	−82.7	−87.9	−0.26±0.08

cm/mol. After plotting against J the BIs of all the lines in a band together with their standard deviations, we discard those with large deviation from the mean and average the remaining ones to obtain an overall BI value.

During the completion of this work, we realized that the purity of the HCN sample we were using was questionable. We make HCN by reacting stearic acid with KCN in vacuum. Since the stearic acid is a wax at room temperature, we can easily control the reaction by changing the temperature. It turns out that together with HCN, some CO_2 is produced. Another problem that we recognized too late is that the HCN is absorbed or polymerizes quickly on the walls of the RDC cell. In fact, we could notice that after filling the cell, the pressure would decrease appreciably over a span of several hours. Consequently, we repeated our measurements in more accurately controlled conditions. We eliminated the CO_2 impurity almost completely by freezing the sample at −100 °C and pumping on it. To compensate for the decreasing pressure during data collection, we built an accurate control circuit that reads the pressure gauge (MKS Baratron capacitance manometer, 100 Torr full scale, 0.5% accuracy) and opens an electromagnetic valve to deliver additional HCN when needed. Among others minor modifications, we changed the PMT (Hamamatzu R268) and we employed a new set of mirrors for the 105 and 006 overtones. We find 10%–20% agreement with the previous intensities for the 105, 006, 205, 106, and 007 overtones. However, for the 305, 206, and 107 overtones, the new values are twice as large as the old ones. This is explained by noting that these three bands had been measured with a cell filled two days before (we would close the cell and assume that the pressure would remain constant).

We believe that the discrepancies with the previous measurements should be mostly attributed to sample impurities and pressure changes, but we have noticed that other factors can produce large errors in the intensity determination. Besides the ASE much care must be taken in the choice of parameters such as the windows delay Δt, the window duration (which must be equal for both windows), and the window integration time constant. In particular, if Δt is too large, the second window integrates over an almost vanishing decay signal and the result is very sensitive to any small offset of the baseline. This may produce an enhancement or a suppression of the absorption signal depending on the offset being negative or positive (assuming a positive decay signal).

In the most recent measurements, we find that the repeatability for the band intensities is better than 5%. This uncertainty is quite larger than the intrinsic standard deviation of the single data sets and we do not have any explanation for these residual systematic errors.

In Table III, we list the BIs for all the measured bands, except the very noisy 117←010 hot band. These values are the ones obtained from the last set of measurements, as explained in the previous paragraph. We checked for a linear Herman–Wallis[23] J dependence for the BIs of the single lines, without finding anything significant. Also listed are the intensities recently calculated by

TABLE III. Intensities of the measured HCN overtone bands. These values are obtained by averaging the band intensities of all strong lines in each band. The error bar on these values is on the order of 5%, which corresponds to the repeatability that we have observed. *Ab initio* values by Botschwina (Ref. 22) are reported in the third column. In the fourth column, we list values calculated by us from the potential of Carter (Refs. 9 and 20) (the same as that used for the rotational constants in Table II, but restricted to stretches only), using the *ab initio* dipole function by Botschwina (Refs. 10 and 12) and basically his same procedure. In the last column are results based on three potentials fitted to the same data by McCoy and Sibert. The labeling of these potentials (f,g,h) is the same as in their paper (Ref. 25).

Transition	Expt. (cm/mol)	Botschwina	Carter–Mills	McCoy–Sibert		
				f	g	h
105←000	3.51	4.53	5.3	4.9	4.0	6.8
006←000	2.61	2.88	3.4	3.1	2.6	4.3
205←000	0.58	0.39	0.56	0.45	0.29	0.66
116←010	0.78	-	-			
106←000	0.89	0.69	0.94	0.79	0.56	1.15
007←000	0.55	0.28	0.40	0.33	0.24	0.47
305←000	0.092	0.026	0.052			
206←000	0.22	0.092	0.16	0.12	0.06	0.17
107←000	0.24	0.098	0.17	0.12	0.07	0.18

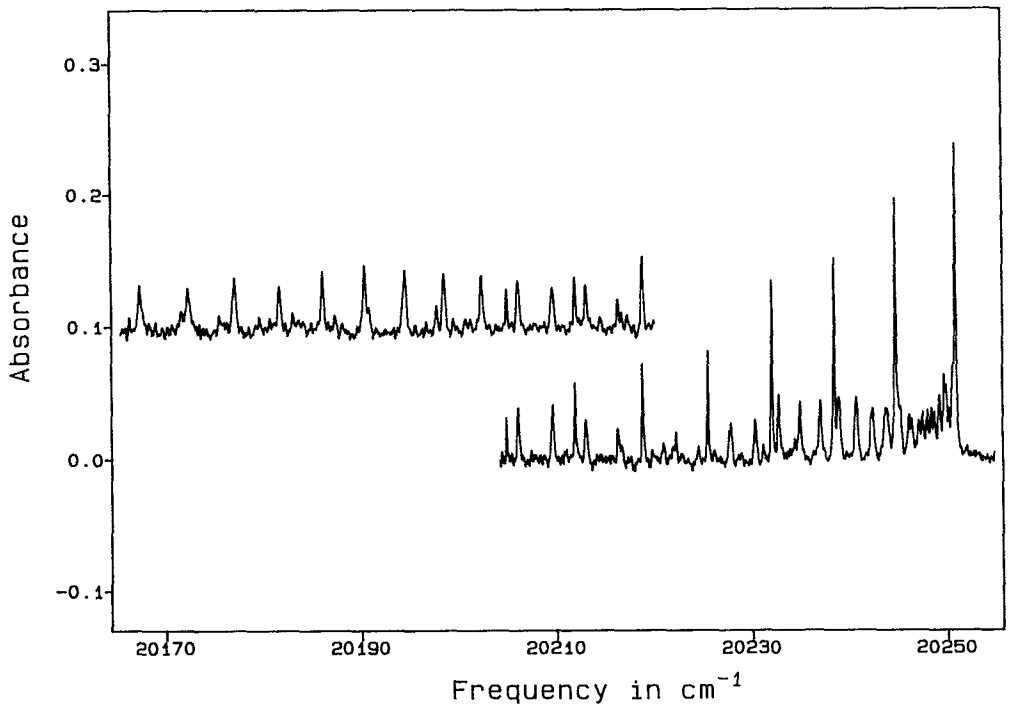

FIG. 8. The 116←010 HCN hot band obtained in the conditions of Fig. 6. Numerical smoothing was used to improve readability of the spectrum. The strong and sharper lines progressing from right to left belong to the tail of the 106 *P* branch.

Botschwina,[22] obtained from an *ab initio* two-dimensional potential for the stretching degrees of freedom using a very large basis set formed by products of harmonic oscillator functions for the two stretching normal coordinates.[12] Except for the higher overtones, the agreement with the experimental values is excellent, especially considering the large sensitivity of calculated intensities to variations in the potential energy surface.[24] In the same table are listed values calculated by us with the potential of Carter *et al.*,[9,20] restricted to stretches only. This empirical energy surface is the same used by Carter *et al.* to calculate the band origins and the rotational constants reported in Tables I and II. As a dipole function, we used the *ab initio* one by Botschwina[10,12] and we followed his same procedure including the correction for the neglected bending motion (see also Smith *et al.*[24]). These values are somewhat worse than Botschwina's results in the case of six vibrational quanta, but perform better elsewhere. Finally we report intensities calculated from three potentials fitted to the same experimental data set by McCoy and Sibert. The labeling of these potentials (*f*, *g*, and *h*) is the same as in their paper.[25] Again, except for the overtones with six quanta, we notice that the potential labeled as "*h*" gives very realistic values.

In Fig. 8 we show the 116←010 hot band spectrum after convolution with a smoothing filter. The strong lines in this spectrum belong to the tail of the *P* branch in the 106 band. The *l*-type line splitting is partially resolved only close to the bandhead, where line congestion makes it more difficult to assign the peaks. We were not able to extract any information about the Δq parameter for this hot band and we fitted the center frequencies of the doublets to a regular rotational progression. The parameters of the lower level were constrained to the known values.[19] The intensity of this hot band appears to be equal (Table III) to that of the 106 band if one considers the large error bars. We also detected the 117←010 hot band at the limit of our sensitivity and we could recognize enough lines to be able to assign them and make the rotational fit. The line positions were determined with the aid of a peak find routine. For this hot band, the signal/noise was too low for a meaningful intensity analysis.

The present result for the intensity of the 006 band (2.6 cm/mol) is in good agreement with the earlier measurement, using intracavity photoacoustic spectroscopy (2.4 cm/mol) made by Smith *et al.* The present measurement of the 105 band, however (3.5 cm/mol), gives an intensity significantly lower than either of the two experimental determinations by Smith *et al.* (13.9 and 16.7 cm/mol), but in fair agreement with the predictions of *ab initio* theory (4.53 cm/mol).[12] The first experimental measurement[4] used high resolution, photoacoustic detection, while the second[5] was based on absorption in a traditional White cell with a path length of 466 m. The absorption measurement was done to resolve a conflict with the results of Law and Baggott,[26] who had determined the relative intensities of the 105 and 006 bands using low resolution, photoacoustic spectroscopy. Law and Baggott had determined a relative intensity in good agreement with the *ab initio* prediction.

The second determination of the 105 band intensity by Smith *et al.* was claimed to be definitive, yet is a factor of

4.6 larger than the present value. The difficulty with that measurement was the inadequate path length used, which was the maximum that was practical with the traditional White cell employed. The features attributed to the lines of the 105 band only had peak absorption of a few percent. In retrospect, one is tempted to attribute them to interference fringes, yet the intensity in that study was checked at several pressures and the determined line intensity did scale linearly with pressure. The exact cause of the experimental artifacts that caused such a severe overestimate of the band intensity cannot be determined at this late date, but this experience points to the importance of obtaining adequate path length. Since the ring-down cavity cell provides a limiting path length that is ~ 100 times larger than for the White cell, it is obviously superior for absorption measurements of weak bands.

With the correction of the 105 band, and the addition of even higher excited states, the remarkable agreement of the experimental and *ab initio* intensities is made even more striking. Except for a few clear resonances, the band intensity falls smoothly as one increases either the number of quanta in ν_1 or ν_3. If one looks at the intensity distribution inside of a "polyad" of states with n_1+n_3 =constant, one also sees a smooth trend. At low total quanta, the largest intensity is found in the pure overtone of ν_3, which is predominantly a C–H stretching mode. But starting at six total quanta, the maximum intensity shifts to the combination bands, an effect that gets more pronounced as one goes higher in energy. This trend is predicted almost quantitatively by the *ab initio* calculations. In the earlier work of Smith *et al.*, it was pointed out that such a shifting of intensity is expected from the simple fact that ν_3 is not a pure C–H stretching mode. In the harmonic limit, the relative intensity inside a polyad should follow a binomial distribution if one makes the bond dipole approximation. It was found, however, that the mixing of the harmonic normal modes was not large enough to reproduce the amount of intensity mixing that was predicted by the *ab initio* calculation. The fault was then laid[4] on the bond dipole approximation, due largely to the fact that the *ab initio* dipole function of Botschwina had cross terms in a Taylor expansion as large as the diagonal terms, thus implying that a bond dipole function [of the form $\mu=\mu_1(r_{CH})+\mu_2(r_{CN})$] is a poor approximation. Subsequently, however, Botschwina showed that dropping the off-diagonal terms in his dipole expansion (which results in the bond dipole form) changed the predicted intensities by only a slight amount.[4]

At least part of the explanation of this "anomaly" is, as pointed out by Fleming and Hutchinson,[27] that the "optimal modes" at such high energy are rotated away from the harmonic modes. Since with increasing energy, the CH bond falls in effective vibrational frequency, it tunes closer to resonance with the CN mode. Thus unlike the situation in symmetric hydrides, the CH oscillator becomes a poorer "local mode" as the excitation is raised. In fact, using the Morse parameters for the CH and CN modes, one predicts that the CH mode will tune into an exact 1–1 resonance with the CN mode near $n_{CH}=9$.

We thus see that the extensive mixing of intensity between the C–H and C–N stretching modes is not a consequence of "energy transfer,"[28] but of a redefinition of the effective modes. The other obvious feature of the spectrum is the clear absence of any bands involving excitation of the bending mode. This implies that there must be no significant mixing of the pure stretching states with those possessing some degree of bending excitation. The highest observed level has an energy 0.5 eV higher than the predicted isomerization barrier to HNC, yet the energy stays locked in the stretching modes and no isomerization can occur.

The recent empirical force field of Carter, Handy, and Mills[9] also predicts that the presently observed states are represented by simple wave functions dominated by single basis functions. In order to illustrate this point, we have used the most recent version of their potential[20] and the same procedure we referenced above with regard to the BI's calculations, and we found the eigenvalues and wave functions in a basis of product Morse functions. For the observed states, contour plots of the wave functions are shown in Fig. 9. In each case, assignment of the quantum numbers of the states based on nodal lines is obvious. This demonstrates without doubt the simplicity of the vibrational dynamics of HCN even at energies exceeding the isomerization barrier and over 50% of the CH dissociation energy.

HCN may well be unique in its near absence of substantial perturbations to the spectrum, even at such high energy. An intriguing question is for how much higher in energy will this behavior persist. Order in the spectrum can break down in two ways. First, the regions of 1–1 and 3–2 resonances of the CH and CN stretching modes could overlap, leading to chaotic energy exchange between the two oscillators. Given the small strength of the 3–2 resonance, such an effect will likely be limited to a small number of states and thus may be difficult to interpret in the spectrum. Much more dramatic would be a resonant coupling with the bending mode. This will greatly increase the density of observable states in the spectrum and eventually will lead to isomerization of the molecule when the mixing becomes strong enough. The question is at what energy will this occur?

V. CONCLUSION

It is clear from the discussion regarding the HCN 105 overtone band intensity that the advantage of the RDC detection scheme over the photoacoustic technique lies in the accuracy of the absolute intensity values since the sensitivity is approximately of the same order of magnitude. Time resolved, intracavity loss spectroscopy has also been demonstrated to provide accurate absorption coefficients[29] and sufficient sensitivity. However, this method is much more expensive and difficult to implement in comparison with RDC. In particular, we have demonstrated that the use of a boxcar to process the data simplifies the RDC scheme without degrading its sensitivity. The high reflectivity mirrors are quite inexpensive if they are available "off the shelf," while custom coating costs in the range of few thousand dollars. The spectral coverage is very wide

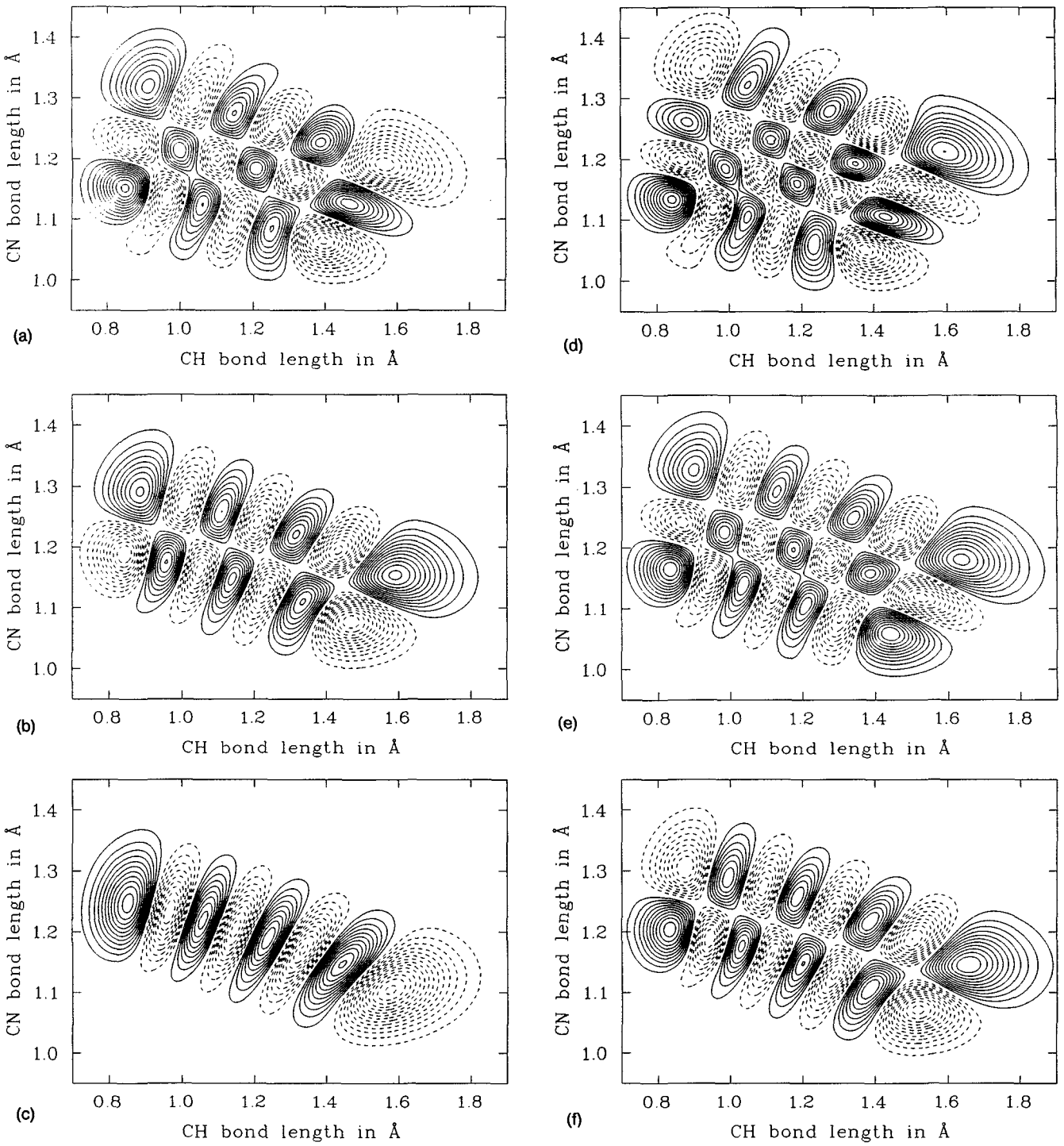

FIG. 9. Contour plots of the wave functions of the stretches for the observed HCN overtones. These are calculated from the most recent potential fit by Carter, Handy, and Mills (Ref. 20), which includes most of the experimental data available. The wave functions are easily identified by counting the nodal planes (a) 205; (b) 106, (c) 007; (d) 305; (e) 206; (f) 107.

and is principally determined by the availability of high quality mirrors. At the blue end of the visible spectrum, mirror losses start to become the limiting factor, and the present practical limit can be probably placed in the range 300–350 nm. At the red end, the limit is constituted by the availability of powerful pulsed laser sources. As is clear from our discussion, the ultimate sensitivity of the RDC technique is directly proportional to the square root of the laser pulse intensity and inversely to the mirrors' total losses ($\mathcal{T}+\mathcal{L}$). If several pulses are averaged for each data point, then the laser duty cycle should be considered rather than the pulse intensity alone.

The simplicity of the RDC makes it a promising candidate for application in different fields, as it has already

been the case for the pulsed molecular beam metal cluster absorption spectroscopy recently pioneered by O'Keefe *et al.*[30] The RDC scheme should be considered for applications that require time resolved (on a time scale longer than 100 μs) and frequency selected measurement of small absorption cross sections or spectrally intense, but very diluted species.

With respect to HCN, we have repeated the same overtone measurements on the isotopomers $HC^{15}N$ and $H^{13}CN$, and the results will be reported soon. In $HC^{15}N$, all of the measured overtone bands are unperturbed except the 206. A combination differences analysis shows clearly that this overtone is in resonance with other two bands. By comparing with accurate band origin predictions by Carter *et al.*,[20] it has been possible to assign the quantum numbers of the perturbing states. In fact, the three experimental band origins match the ones calculated for the 206, 802, and 02°7 states with a systematic error of $+1$ cm^{-1}.

It is surprising that HCN does not show any sign of chaotic dynamics when the linear degrees of freedom of the molecule are excited well above the isomerization energy. This suggests that the coupling of the stretching and bending coordinates in HCN is very marginal and might explain the success of those simplified theoretical models which involve only the two stretch modes.[10,24]

ACKNOWLEDGMENTS

We would like to thank J. C. Bergquist for lending us one of the high reflectivity mirrors set; I. M. Mills, S. Carter, N. C. Handy, P. Botschwina, B. Gazdy, and J. M. Bowman for sharing with us the latest results of their calculations. We also acknowledge Alice Smith, who provided the programs used to calculate the wave functions and the vibrational transition strengths reported here. Technical suggestions by Ramin Lalezari were also very useful. Funding was provided by the Donors of the Petroleum Research Fund, administered by the American Chemical Society.

[1] K. K. Lehmann and A. M. Smith, J. Chem. Phys. **93**, 6140 (1990).
[2] K. K. Lehmann, G. J. Scherer, and W. Klemperer, J. Chem. Phys. **77**, 2853 (1982).
[3] A. M. Smith, K. K. Lehmann, and W. Klemperer, J. Chem. Phys. **85**, 4958 (1986).
[4] A. M. Smith, U. G. Jørgensen, and K. K. Lehmann, J. Chem. Phys. **87**, 5649 (1987).
[5] A. M. Smith, W. Klemperer, and K. K. Lehmann, J. Chem. Phys. **90**, 4633 (1989).
[6] A. M. Smith, S. L. Coy, W. Klemperer, and K. K. Lehmann, J. Mol. Spectrosc. **134**, 134 (1989).
[7] H. Sasada, J. Chem. Phys. **88**, 767 (1988).
[8] X. Yang, C. A. Rogaski, and A. M. Wodtke, J. Chem. Phys. **92**, 2111 (1990); X. Yang and A. M. Wodtke, *ibid.* **93**, 3723 (1990); X. Yang, C. A. Rogaski, and A. M. Wodtke, J. Opt. Soc. B **7**, 1835 (1990).
[9] S. Carter, N. C. Handy, and I. M. Mills, Philos. Trans. R. Soc. London Ser. A **332**, 309 (1990).
[10] P. Botschwina, J. Chem. Soc. Faraday Trans. 2 **84**, 1263 (1988).
[11] A. O'Keefe and D. A. G. Deacon, Rev. Sci. Instrum. **59**, 2544 (1988).
[12] P. Botschwina, Chem. Phys. **81**, 73 (1983).
[13] J. M. Herbelin, J. A. McKay, M. A. Kwok, R. H. Ueunten, D. S. Urevig, D. J. Spencer, and D. J. Benard, Appl. Opt. **19**, 144 (1980).
[14] D. Z. Anderson, J. C. Frisch, and C. S. Masser, Appl. Opt. **23**, 1238 (1984).
[15] A. Yariv, Quantum Electronics, 3rd ed. (Wiley, New York, 1989).
[16] *CRC Handbook of Chemistry and Physics*, 67th ed., edited by R. C. Weast (Chemical Rubber Co., Boca Raton, FL, 1986).
[17] Mr. R. Lalezari, Particle Measurement Systems, Electro Optics Division, Boulder, CO 80301.
[18] G. Rempe, R. J. Thompson, H. J. Kimble, and R. Lalezari, Opt. Lett. **17**, 363 (1992).
[19] A. G. Maki, W. B. Olson, and R. L. Sams, J. Mol. Spectrosc. **36**, 433 (1970).
[20] S. Carter, N. C. Handy, and I. M. Mills, J. Chem. Phys. (to be published).
[21] B. Gazdy and J. M. Bowman, J. Chem. Phys. **95**, 6309 (1991).
[22] P. Botschwina (private communication).
[23] R. Herman and R. F. Wallis, J. Chem. Phys. **23**, 637 (1955).
[24] A. M. Smith, W. Klemperer, and K. K. Lehmann, J. Chem. Phys. **94**, 5040 (1991).
[25] A. B. McCoy and E. L. Sibert III, J. Chem. Phys. **97**, 2938 (1992); the intensities we report constitute a private communication.
[26] J. E. Baggott and D. W. Law, J. Chem. Soc. Faraday Trans. 2 **84**, 1560 (1988).
[27] P. R. Fleming and J. S. Hutchinson, J. Chem. Phys. **90**, 1735 (1989).
[28] W. Quapp, J. Mol. Structure **218**, 261 (1990).
[29] F. Stoeckel and G. H. Atkinson, Appl. Opt. **24**, 3591 (1985).
[30] A. O'Keefe, J. J. Scherer, A. L. Cooksy, R. Sheeks, J. Heath, and R. J. Saykally, Chem. Phys. Lett. **172**, 214 (1990).